# Synchronization of semiconductor lasers with coexisting attractors

F. R. Ruiz-Oliveras and A. N. Pisarchik
*Centro de Investigaciones en Optica, Loma del Bosque 115, Lomas del Campestre, 37150 Leon, Guanajuato, Mexico*
(Received 3 October 2008; published 15 January 2009)

We study synchronization of unidirectionally coupled optical bistable systems. In particular, we consider two semiconductor lasers with an external cavity, which exhibit, when isolated, coexistence of two different attractors: fixed point and chaos, fixed point and one periodic orbit, and two periodic orbits with different periods. The analysis is performed with a cross-correlation function between the master and slave laser oscillations calculated with model equations based on the Lang-Kobayashi approach. Depending on both the laser operating point and the coupling strength, different bifurcations (Hopf, period doubling, saddle node, torus, and crisis) and diverse dynamical regimes (steady state, periodicity, quasiperiodicity, bistability, and chaos) occur in the route from asynchronous motion to complete synchronization. We show some similarities and differences between synchronization of monostable and bistable lasers.

DOI: 10.1103/PhysRevE.79.016202 PACS number(s): 05.45.Xt, 42.55.Px, 42.65.Sf

## I. INTRODUCTION

Many dynamical systems, such as electronic circuits [1], lasers [2], mechanical systems [3], turbulent flows [4], biological systems [5], and chemical reactions [6] exhibit coexistence of two or more attractive states for the same values of the system parameters. This phenomenon is referred to as generalized multistability, where the actual state is determined by initial conditions only. In recent years the interest in studying such systems has increased, essentially because of their potential applications as mechanisms for memory storage in artificial and biological neural networks [7].

In spite of numerous works devoted to synchronization phenomena in monostable systems (see, e.g., [8] and references therein), synchronization of systems with coexisting attractors still remains a long-standing and challenging problem with broad interdisciplinary interest; because of the possible applications, a deeper understanding of the fundamental aspects of coherent complex dynamics is needed. The first attempts to attack this problem were made by studying the synchronization of a coupled system where multistability resulted from the coupling due to the increase in the system's complexity [9]. Two different chaotic attractors appeared in mutually coupled identical systems, e.g., Rössler oscillators [10], or in structurally different systems coupled in a master-slave configuration, such as Lorenz and Rössler oscillators [11]. Only recently has synchronization of coupled systems which, being isolated, exhibit the coexistence of attractors been studied [12]. In particular, when two unidirectionally coupled Rössler-like electronic circuits with coexisting chaotic attractors have been used, different types of synchronization (intermittent, phase, anticipated, period-doubling synchronization) have been found in the route from asynchronous motion to complete synchronization as the coupling is increased.

Lasers are among the most convenient dynamical systems for theoretical and experimental studies of synchronization phenomena, as well as for their applications in optical communication networks. Research has been made for synchronization in different types of lasers, e.g., solid state [13], $CO_2$ [14,15], fiber [16], and semiconductor lasers [17]. Semiconductor lasers have attracted more attention due to their direct compatibility with existing optical fiber communications technology (see, e.g., [18] and references therein). Moreover, semiconductor lasers have a particular feature that distinguishes them from other types of lasers: its relaxation oscillation frequency is usually very high (several gigahertz), which is approximately four orders of magnitude higher than the fundamental frequencies of gas, solid-state, and fiber lasers; this makes semiconductor lasers excellent optical devices for fast information transmission. This feature enables complex dynamics to appear when two semiconductor lasers are coupled, even if both were operating in a steady-state regime when isolated, because, when a small detuning of their optical frequencies interacts with the laser relaxation oscillation frequency, the system often goes through regions of bifurcations and chaos. In fact, the frequency detuning acts as an additional degree of freedom in the coupled system. It was shown first theoretically [17] and then confirmed experimentally [19] that unidirectionally coupled chaotic semiconductor lasers with optical feedback can be synchronized and used in encoded communications systems. Complete synchronization is achieved when the lasers are well matched, i.e., when they operate at the same lasing frequencies.

Like any other complex dynamical systems, lasers can display coexistence of attractors. The first experimental evidence of multistability in lasers was demonstrated by Arecchi *et al.* [20] in a loss-modulated $CO_2$ laser. Later, multistability was detected in other lasers, including a neodymium-doped yttrium aluminum garnet (Nd:YAG) laser with intracavity second-order harmonic generation [21] and a fiber laser [22]. Recently, we have shown that the complex dynamics of an external cavity semiconductor lasers (ECSL) allows coexistence of steady-state, periodic, quasiperiodic, or chaotic attractors [23]. These advantages make ECSLs excellent candidates for studying synchronization phenomena in coupled multistable systems. The description of the dynamical behavior of such lasers usually requires delay differential equations [24], where the delayed feedback is responsible for the complexity emergence, in particular, multistability [25,26].

 

TABLE I. Parameters used in simulations.

| $\alpha$ | $g$ | $N_0$ | $s$ | $\tau_p$ | $\tau_n$ | $\tau_c$ | $I$ | $e$ | $R$ |
|---|---|---|---|---|---|---|---|---|---|
| 3 | $1.5\times10^{-8}$ ps$^{-1}$ | $1.5\times10^{8}$ | $10^{-7}$ | 2 ps | 2 ns | 6.6 ps | 29 mA | $1.6\times10^{-19}$ C | 0.3 |

In the last two decades, the ECSL dynamics has been extensively studied due to the important applications in interferometric sensors, chaotic optical communication, etc. (see [27] and references therein). Such parameters as feedback strength, feedback length, and wave initial phase in the external cavity can be used as control parameters to obtain different dynamical regimes, including periodic and quasiperiodic oscillations, low-frequency chaotic fluctuations, and coherent collapse. Recently, we have shown that the dynamics of a semiconductor laser with two external cavities could be adequately controlled by properly adjusting both the length and the feedback strength of the external cavities [23]. The analysis of codimensional-2 state diagrams of ECSLs has demonstrated that steady states and different periodic orbits can be locked at some rational multiple of the phases of the external cavities, forming Arnold tongue structures in the parameter spaces of the external cavity length, feedback strength, and pump parameter. Phase-locking methods are of great significance in optics, and often used to improve the light intensity [28,29]. Furthermore, we have demonstrated that a laser with a very long external cavity is always unstable [23]. The common occurrence of such behavior in feedback systems has been confirmed both theoretically and experimentally for different types of lasers. For example, in $CO_2$ lasers coupled in an axisymmetricfold configuration, various cavities were phase locked when the curvature radius of the control mirror front surface was properly adjusted [28]. Recently, an integrated device composed of a semiconductor laser and a double cavity has been proposed for chaos-based communications [30]. Modern studies of a periodically driven semiconductor laser subject to optical feedback from a microcantilever demonstrated the interspike behavior of the light intensity, which has a potential application for resonant sensing [31].

This paper is devoted to a detailed numerical study of the ECSL dynamics and synchronization of two identical ECSLs in a master-slave configuration. First we study synchronization of monostable lasers, i.e., when each laser has a single attractor. Then we investigate the case when two lasers, being isolated, each exhibit the coexistence of two different attractors, some combination of fixed points, periodic or chaotic orbits. We address our research to the general problem: When coupled, how do these multistable lasers synchronize? Which of the coexisting attractors is selected or how does the coupling strength affect the coupled system? What types of bifurcations appear in the coupled system and what route from asynchronous motion to complete synchronization is chosen for different coexisting attractors?

The rest of the paper is organized as follows. In Sec. II we describe the laser model and study dynamics of a single ECSL by analyzing its bifurcation diagrams in one, two, and three dimensions. We show a very rich dynamics including coexistence of different attractors. To reveal the features inherent in coupled multistable systems we first consider in Sec. III laser synchronization in the monostability regions and then, in Sec. IV, we study synchronization in different bistability regions and compare the results with those obtained for monostable lasers. Finally, the main conclusions are given in Sec. V.

## II. DYNAMICS OF AN EXTERNAL CAVITY SEMICONDUCTOR LASER

### A. Model equations

ECSLs can be modeled by the following equations based on the well-known Lang-Kobayashi approach [17,24]:

$$\dot{E}_m(t) = (1+j\alpha)\left(\frac{g(N_m(t)-N_0)}{1+s|E_m(t)|^2} - \frac{1}{\tau_p}\right)\frac{E_m(t)}{2} + \kappa E_m(t-\tau)\exp(-i\varphi), \tag{1}$$

$$\dot{N}_m(t) = \frac{I}{e} - \frac{N_m(t)}{\tau_n} - \frac{g(N_m(t)-N_0)}{1+s|E_m(t)|^2}|E_m(t)|^2, \tag{2}$$

where the subscript $m$ stands for the master laser, $E(t)$ is the amplitude for the slowly varying complex electrical field, $|E_m|^2=P_m$ is the optical power in terms of the number of photons, $N(t)$ is the carrier number, $\alpha$ is the linewidth enhancement factor, $g$ is the gain parameter, $N_0$ is the carrier number at transparency, $s$ is the gain saturation coefficient, $\tau_p$ and $\tau_n$ are the photon and carrier lifetimes respectively, $\kappa=[(1-R)/\tau_c]\sqrt{R_{\text{ext}}/R}$ is the feedback strength, $\tau$ is the external cavity round-trip time, $R$ and $R_{\text{ext}}$ are the facet power reflectivities of the laser and of the feedback external mirror, $\varphi\in[0,2\pi]$ is the phase, $I$ is the bias current (the laser threshold current $I_{\text{th}}=14.7$ mA), and $e$ is the electron charge. Table I shows the simulation fixed parameters, the parameters $\kappa$, $\tau$, and $\varphi$ are varied for every specific case considered in this paper to construct codimensional-one, -two, and -three bifurcation diagrams.

## III. BIFURCATION DIAGRAMS

As we said before, the dynamics of a solitary ECSL has been extensively studied; for moderate and strong feedback strengths ECSL displays a very complex dynamical behavior, from steady states and periodic orbits to quasiperiodicity and chaos [23,32,33]. Moreover, for some parameters, an ECSL exhibits coexistence of different attractors [34]. This phenomenon can be found through codimensional-1 bifurcation diagrams, such as presented in Fig. 1. By taking different initial conditions, we encounter regions of coexistence of a continuous wave (cw) regime (fixed point) with chaos (CH), cw with a period 2 (P2) attractor, and a period-1 (P1) with a P2 attractor. In our laser and, in the parameters range we

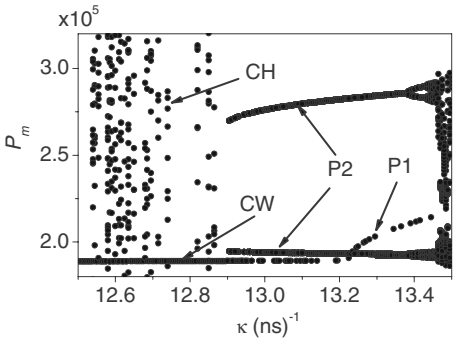


FIG. 1. Bifurcation diagram of laser peak power as a function of feedback strength demonstrating coexistence of different attractors. $\phi=\pi$ and $\tau=0.4$ ns$^{-1}$.

used, we were unable to find the coexistence of different chaotic regimes, as in the Rössler oscillator [12].

To better understand the ECSL dynamics, we also construct the three-dimensional (3D) bifurcation diagram using $\phi$, $\kappa$, and $\tau$ as control parameters, shown in Fig. 2. For small feedback strengths ($\kappa \leqslant 7.5$ ns$^{-1}$), the dynamics of the ECSL has a regular behavior (steady states and periodic orbits), whereas for a larger feedback ($\kappa > 7.5$ ns$^{-1}$) the laser becomes involved in an irregular motion, such as quasiperiodicity and chaos. In the 3D bifurcation diagram in Fig. 2, the boundaries between black and yellow regions are the Hopf bifurcation surfaces, between yellow and blue regions are the period-doubling bifurcation surfaces, and between yellow and white regions are either torus or crisis bifurcation surfaces.

Three selected slices of the 3D diagram, taken each in different directions, are shown in Fig. 3 and represent the codimensional-2 bifurcation diagrams, where we fix $\kappa = 10$ ns$^{-1}$ [Fig. 3(a)], $\tau=0.25$ ns [Fig. 3(b)], and $\phi=0$ [Fig. 3(c)]. These 2D diagrams display a $2\pi$-periodic structure with respect to phase $\phi$ in good agreement with previous findings [23,34].

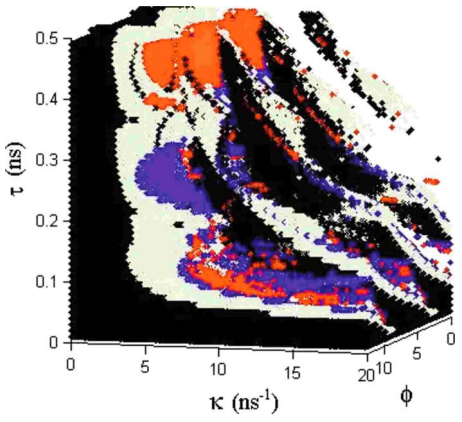


FIG. 2. (Color online) Laser state diagram in 3D parameter space of feedback strength, feedback length, and external round-trip time. The fixed points are shown in black, period 1 in green (light gray), period 2 in blue (dark gray), period 3 in red (gray), and quasiperiodic or chaotic orbits in white. See [37] for a movie corresponding to this figure.

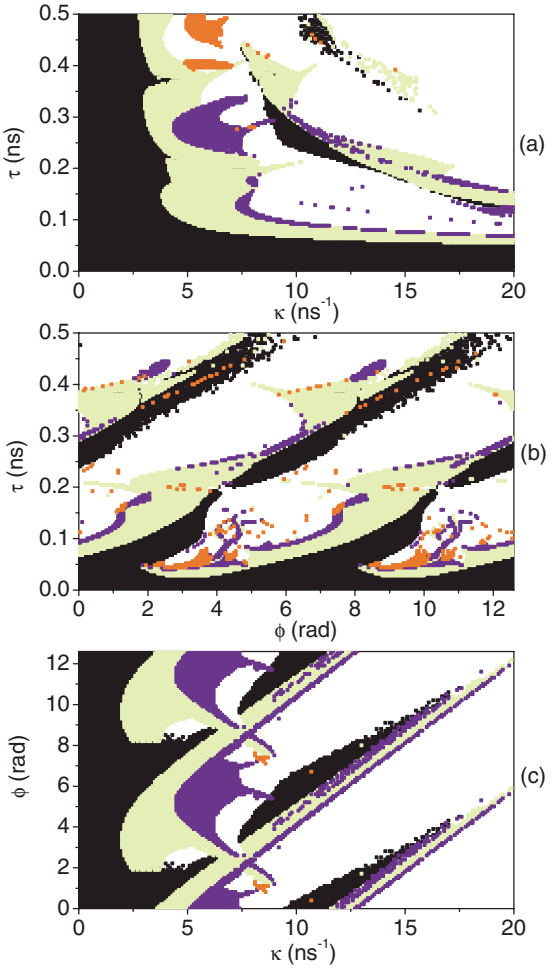


FIG. 3. (Color online) Codimensional-2 bifurcation diagrams in parameter spaces of (a) $\kappa$ and $\tau$ for $\phi=2\pi n$ ($n=0, \pm 1, \pm 2, \ldots$), (b) $\phi$ and $\tau$ for $\kappa=10$ ns$^{-1}$, and (c) $\kappa$ and $\phi$ for $\tau=0.25$ ns.

## IV. COUPLED LASERS IN MONOSTABILITY REGIONS

We start our research on synchronization with the case of coupled ECSLs in monostability regions, to be able later on to compare its features with those inherent to multistable systems. In this section, we consider three different cases: uncoupled ECSLs operating in a monostable steady-state (fixed point), periodic, and chaotic regimes.

### A. Model equations for slave laser

The system of two identical unidirectionally coupled ECSLs can be modeled by four differential equations, two for the master laser (ML) [Eqs. (1) and (2)] and two for the slave laser (SL). The equations for the SL can be written as follows:

$$\dot{E}_s(t) = (1 + j\alpha)\left(\frac{g(N_s(t) - N_0)}{1 + s|E_m(t)|^2} - \frac{1}{\tau_p}\right)\frac{E_s(t)}{2} + \kappa E_s(t-\tau)\exp(-i\varphi) + \gamma E_m(t)\exp(-j\delta_w t), \quad (3)$$

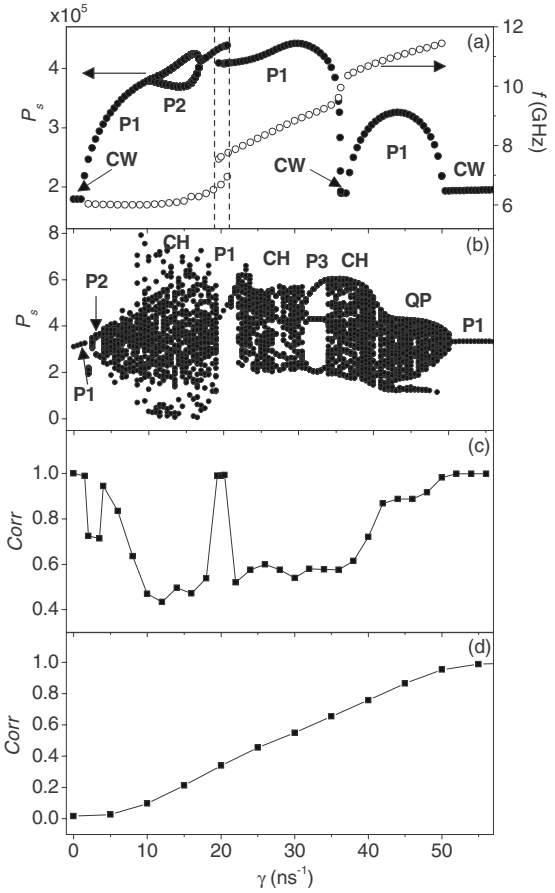


FIG. 4. Dynamics of coupled monostable lasers. (a) Bifurcation diagram of SL peak power when uncoupled lasers are in a steady-state regime; (b),(c) bifurcation diagram and cross correlation between ML and SL when both lasers are in a period-1 regime; and (d) cross correlation between ML and SL when both lasers are in a chaotic regime. The dashed lines bound the region of coexistence of two periodic orbits with different frequencies.

$$\dot{N}_s(t) = \frac{I}{e} - \frac{N_s(t)}{\tau_n} - \frac{g(N_s(t) - N_0)}{1 + s|E_s(t)|^2}|E_s(t)|^2, \tag{4}$$

where the subscript $s$ stands for SL, $\delta_w$ is the detuning between the optical frequencies of the free-running ML and SL (for simplicity, we consider $\delta_w = 0$), and $\gamma$ is the coupling strength related to the injected field from the ML into the SL ($\gamma = 50$ ns$^{-1}$ corresponds to the case when approximately 22% of the ML output power is injected into the SL). The parameters $\kappa$, $\tau$, $\varphi$, and $\gamma$ are varied for every specific case considered in this paper.

### B. Steady-state regime

First, we consider the case when both lasers are isolated and operate in a monostable cw regime. This regime can be found for $\kappa = 2.5$ ns$^{-1}$, $\tau = 0.43$ ns, and $\varphi = 0$. It is known that moderate optical injection induces various bifurcations in the SL, such as Hopf, period-doubling, and saddle-node bifurcations [35]. Figure 4(a) shows the bifurcation diagram of the SL peak power as a function of the coupling parameter $\gamma$. In the same figure, we plot the frequency $f$ of the laser oscillations.

As $\gamma$ is increased, the dynamics of the SL is characterized by the following bifurcations.

(1) Steady-state emission (cw) ($\gamma < 1$ ns$^{-1}$).

(2) Hopf bifurcation at $\gamma \approx 1$ ns$^{-1}$ leading to periodic oscillations (P1) with relaxation oscillation frequency $f \approx f_r = 6$ GHz ($1 < \gamma < 10$ ns$^{-1}$).

(3) Forward period-doubling bifurcation at $\gamma \approx 10$ ns$^{-1}$; the first-order harmonic of the oscillation frequency $f$ increases as $\gamma$ is increased within $10 < \gamma < 20$ ns$^{-1}$.

(4) Backward period-doubling bifurcation at $\gamma \approx 17.5$ ns$^{-1}$ leading to P1; $f$ continues to increase with $\gamma$.

(5) Saddle-node bifurcations at $\gamma \approx 19.7$ and 21 ns$^{-1}$ leading to the coexistence of two P1 regimes with different frequencies $f_1$ and $f_2$; $f_2$ increases linearly with $\gamma$.

(6) Inverse Hopf bifurcation at $\gamma \approx 36.3$ ns$^{-1}$; the peak power rapidly decreases as $\gamma$ approaches this bifurcation point, resulting in steady-state emission within $36.3 < \gamma < 37$ ns$^{-1}$.

(7) Another Hopf bifurcation at $\gamma \approx 37$ ns$^{-1}$ leading to periodic oscillations with higher $f$, linearly increasing up to double the relaxation oscillation frequency $f \approx 2f_r$.

(8) Another inverse Hopf bifurcation at $\gamma \approx 50.5$ ns$^{-1}$ resulting in steady-state emission.

One can see that, even in this relatively simple case of the coupled cw ECSLs, the dynamics is rather complicated. Previous studies of optical injection in semiconductor lasers without an external cavity have also underlined the complex behavior; however, the oscillations have been observed only with frequencies corresponding to the offset of the beating between the laser frequency and the frequency of the injected light [36]. It is of special interest that in the case of ECSLs the oscillation frequency depends on the coupling parameter. Another interesting observation is that a moderate coupling of two identical cw ECSLs can induce bistability (in our case, periodic regimes with different frequencies).

### C. Periodic regime

Now consider the case when both ML and SL are in a periodic regime. A period-1 regime is realized for the following parameters: $\kappa = 4$ ns$^{-1}$, $\tau = 0.4$, and $\varphi = \pi$. The bifurcation diagram of the peak SL power versus the coupling strength shown in Fig. 4(b) displays a very rich synchronization dynamics: period 1 (P1), period 2 (P2), quasiperiodicity (QP), and chaos (CH) with periodic windows (P3) are observed for different values of $\gamma$. To quantitatively measure synchronization, we calculate the normalized cross correlation Corr between the ML and SL output powers:

$$\mathrm{Corr}(t) = \frac{\langle [P_m(t')P_s(t'-t) - \overline{P_m P_s}] \rangle_{t'}}{\sigma_m \sigma_s}, \tag{5}$$

where $\langle \cdots \rangle$ stands for the time average, and $\overline{P_m}$, $\overline{P_s}$ and $\sigma_m$, $\sigma_s$ are the means and standard deviations of the ML and SL powers, respectively. In this paper we take into consideration only isochronous synchronization, i.e., we calculate Corr(0). The cross correlation between ML and SL versus $\gamma$ is shown

in Fig. 4(c). As the coupling is increased, the synchronization dynamics goes through the following stages.

(1) P1 orbit, complete correlation ($\gamma < 1.5$ ns$^{-1}$).

(2) Period-doubling route to chaos; Corr decreases with $\gamma$ and reaches its minimum value in the chaotic regime at $\gamma \approx 12$ ns$^{-1}$.

(3) Crisis at $\gamma \approx 19.5$ ns$^{-1}$ followed by fully correlated P1 which in turn also undergoes the period-doubling bifurcation at $\gamma \approx 21$ ns$^{-1}$.

(4) Inverse crisis bifurcation (at $\gamma \approx 22$ ns$^{-1}$) resulting in chaos; weak correlation.

(5) Another crisis (at $\gamma \approx 31$ ns$^{-1}$) followed by a P3 window at $31 < \gamma < 34$ ns$^{-1}$.

(6) Saddle-node bifurcation at $\gamma \approx 34$ ns$^{-1}$ leading to chaos; correlation is improved as $\gamma$ is increased.

(7) Quasiperiodicity with larger correlation ($34 < \gamma < 50$ ns$^{-1}$).

(8) Inverse torus bifurcation at $\gamma \approx 50$ ns$^{-1}$ leading to a strongly correlated P1.

### D. Chaotic regime

Synchronization of monostable chaotic lasers has been extensively studied both numerically and experimentally (see [18] and references therein). First, Mirasso *et al.* [17] showed theoretically that unidirectionally coupled chaotic semiconductor lasers with optical feedback can be completely synchronized, which can be very useful for secure communication systems. Later, Sivaprakasam and Shore [19] experimentally obtained synchronization of chaotic ECSLs. To complete the study of our system, we also consider coupled chaotic lasers. We chose the chaotic regime with the following parameters: $\kappa = 25$ ns$^{-1}$, $\tau = 1$ ns, and $\varphi = \pi$. The cross correlation versus $\gamma$ is shown in Fig. 4(d). Complete synchronization is achieved when $\gamma \geq 60$ ns$^{-1}$.

Thus, the dynamics of coupled monostable ECSLs is very complex, especially for periodically oscillating lasers [Figs. 4(b) and 4(c)], where the moderate coupling induces different types of bifurcations, as well as bistability.

## V. COUPLED LASERS IN BISTABILITY REGIONS

In this section we study synchronization of two bistable lasers, i.e., we begin with the ML and SL uncoupled, operating in different regimes since their initial conditions are different, and change the coupling parameter to study the dynamics of the coupled system. We explore three sets of parameters to get the coexisting attractors shown in Fig. 1. In particular, we find in these regions the coexistence of chaos (CH) with cw, cw with P2, and P2 with P1. Below we will analyze these three cases in detail.

### A. Coexistence of chaos and fixed point

In this bistable regime we fix $\kappa = 12.7$ ns$^{-1}$ (Fig. 1). There are two possible situations dependent on the initial state of the ML and SL: the ML is cw and the SL is chaotic, and vice versa. We consider these two cases separately.

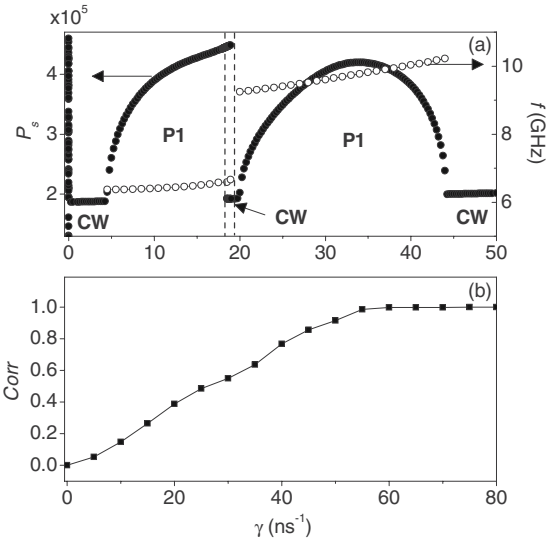


FIG. 5. Dynamics of coupled ECSLs in a bistability region with coexisting chaos and fixed point. (a) Bifurcation diagram of SL peak power when the SL was cw and the ML was chaotic and (b) cross correlation between ML and SL when the SL was chaotic and the ML was cw, as a function of coupling strength. The dashed lines bound the bistability region.

#### 1. cw ML and chaotic SL

Figure 5(a) shows the bifurcation diagram of the SL peak power versus $\gamma$. The dynamics is similar to that for the monostable steady-state lasers [compare with Fig. 4(a)]. Initial chaos in the SL abruptly disappears at very low coupling, giving rise to a cw regime. Then, as in the monostable case, P1 appears in the Hopf bifurcation followed by a bistability region with coexisting P1 and fixed point. This differs from the monostable case where two P1 attractors coexist. Another difference is that we do not observe here the period-doubling bifurcation. The common features are the alternation of the periodic and cw regimes and the bistability region where $f$ jumps from $f_r$ to $2f_r$ as $\gamma$ is increased.

#### 2. Chaotic ML and cw SL

A completely different dynamics is observed when we start out with a chaotic ML and the SL operating in a steady-state regime. Figure 5(b) shows the cross correlation between ML and SL as a function of the coupling parameter. The correlation increases almost linearly as $\gamma$ is increased and the lasers become completely synchronized for $\gamma \geq 60$ ns$^{-1}$. As expected, the dynamics is similar to that of the monostable case when both lasers were chaotic [compare with Fig. 4(d)]. Only a very small amount of radiation injected from the chaotic ML into the cw SL drives the SL trajectory toward the coexisting chaotic attractor; for larger $\gamma$ we now have the case of coupled chaotic lasers.

### B. Coexistence of periodic orbit and fixed point

The coexistence of a P2 orbit with a steady state is observed for $\tau = 0.2$, $\varphi = 0$, and $14.8 < \kappa < 15.5$ ns$^{-1}$. Below we consider two possible variants.

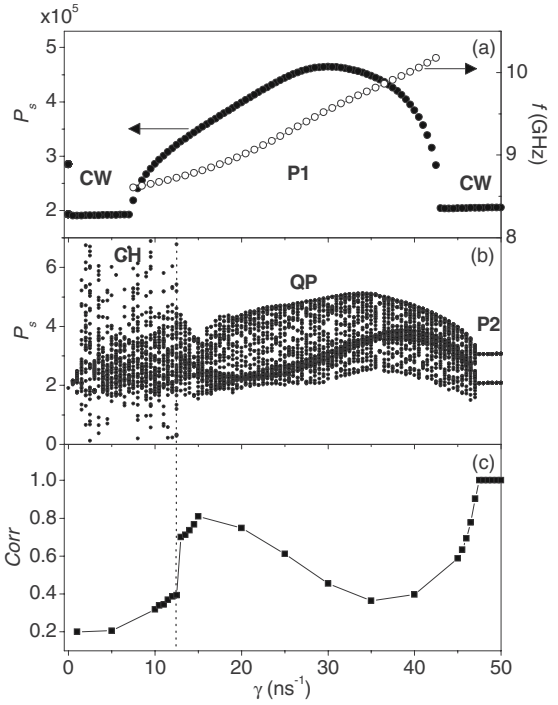


FIG. 6. Dynamics of coupled ECSLs with coexisting fixed point and periodic orbit. (a) Bifurcation diagram of SL peak power when the ML was in the cw and the SL in the P2 regime; (b),(c) bifurcation diagram and cross correlation when the ML was in the P2 and the SL was in the cw regime. The dotted line indicates the boundary between chaotic and quasiperiodic regimes.

#### *1. cw ML and periodic SL*

We first consider the case when the ML is uncoupled and works in a steady-state regime and SL is in P2. In the bifurcation diagram of the SL peak power [Fig. 6(a)], we can see that the P2 regime disappears already at a very weak coupling ($\gamma < 0.5$ ns$^{-1}$), which induces a cw regime. The dynamics is simpler than for the cases considered above, when the ML was also in a steady state [compare with Figs. 4(a) and 5(a)]; here only one P1 region exists between the forward and the inverse Hopf bifurcations, so that the SL stays in a steady state only for small and large $\gamma$; furthermore, no bistability is observed.

#### *2. Periodic ML and cw SL*

The bifurcation diagram for the case when the ML and SL are initially in the P2 and cw regimes, respectively, is shown in Fig. 6(b). The dynamics is very rich: as $\gamma$ is increased, first a chaotic and then a quasiperiodic regime arises, finally to terminate in the inverse torus bifurcation (at $\gamma \approx 47$ ns$^{-1}$) resulting in P2. In Fig. 6(c), one can see how the cross correlation between ML and SL oscillations resembles the dynamics. In general, the correlation with a chaotic regime is weaker than with a quasiperiodic one.

### C. Coexistence of two periodic orbits with different periods

The richest dynamics is observed in the case of coexistence of different periodic regimes. Here we consider the case when P1 coexists with P2 (at $\kappa = 13.3$ ns$^{-1}$, $\tau = 0.3$, and $\varphi = \pi$) as shown in Fig. 1. There are two possible situations.

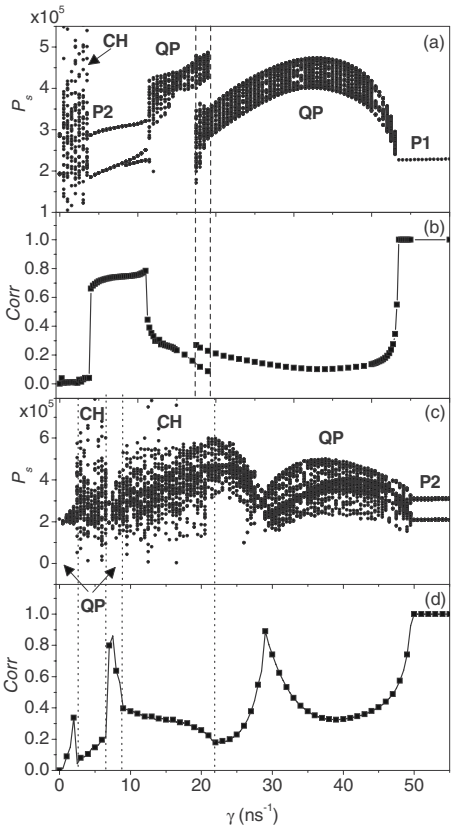


FIG. 7. (a),(c) Bifurcation diagrams and (b),(d) cross correlations of ECSL with coexisting periodic orbits when initially (a),(b) the ML was in P2 and the SL in P1 and (c),(d) the ML in P1 and the SL in P2. Two QP orbits coexist in the range between the two dashed lines. The dotted lines show torus bifurcations.

#### *1. Period-1 ML and period-2 SL*

Figures 7(a) and 7(b) show the bifurcation diagram of the SL peak power and the cross correlation between ML and SL, as functions of the coupling parameter, when the ML initially was in P1 and the SL in P2. For a tiny coupling ($\gamma < 0.5$ ns$^{-1}$), chaos arises, ending in crisis (at $\gamma \approx 3.5$ ns$^{-1}$), followed by P2, which in turn is converted into QP (at $\gamma \approx 11.5$ ns$^{-1}$). Then, as $\gamma$ is further increased, another QP attractor is generated through the saddle-node bifurcation (at $\gamma \approx 17.5$ ns$^{-1}$), which coexists with the previous QP attractor, so that within a certain range of $\gamma$ ($17.5 < \gamma < 19$ ns$^{-1}$) two QP regimes coexist. Finally, at $\gamma \approx 19$ ns$^{-1}$ the first QP disappears, and the second QP continues up to the inverse torus bifurcation (at $\gamma \approx 43.5$ ns$^{-1}$) leading to P1.

#### *2. Period-2 ML and period-1 SL*

Another scenario is observed when the ML initially was in P2 and the SL in P1. Figures 7(c) and 7(d) show the bifurcation diagram and cross correlation for this case. The synchronization dynamics is characterized by a set of torus bifurcations. At a very low coupling, P1 undergoes the first

torus bifurcation (at $\gamma \approx 0.5$ ns$^{-1}$) leading to QP which then is converted into chaos in the second torus bifurcation (at $\gamma \approx 2.5$ ns$^{-1}$). As $\gamma$ is further increased, the laser undergoes the inverse torus bifurcation (at $\gamma \approx 24$ ns$^{-1}$) where chaos is transformed into QP terminated in the second inverse torus bifurcation (at $\gamma \approx 50$ ns$^{-1}$). One can see in Fig. 7(d) that within the QP regions the cross-correlation dependence has a local maximum with Corr $\approx 0.9$. These regions of generalized synchronization are very promising for secure communication with multistable lasers.

## VI. CONCLUSIONS

In this work we have investigated dynamics of two unidirectionally coupled external cavity semiconductor lasers in monostability and bistability regions. The numerical simulations have been performed with a delayed equations model based on the Lang-Kobayashi approach. By analyzing codimensional-1, -2, and -3 bifurcation diagrams in the spaces of the main laser parameters (feedback strength, feedback delay time, and laser field phase), we have shown that the solitary ECSL displays very rich dynamics characterized by diverse bifurcations leading to different dynamic regimes. Within certain parameter ranges, the solitary ECSL exhibits coexistence of different attractors (steady state, periodic, and chaotic) which we explored to study the synchronization of two coupled ECSLs.

The dynamics becomes more complex when two ECSLs are coupled. The analysis has been performed with bifurcation diagrams of the slave laser peak power and the cross correlation function between oscillations of the master and slave lasers, versus the coupling strength. Even in the monostability region, the dynamics of the coupled system is very rich; as the coupling is increased, the trajectory undergoes different bifurcations (Hopf, period doubling, torus, and crisis), giving rise to diverse dynamical regimes (periodic, quasiperiodic, and chaotic) and bistability. To study the region of bistability, one has to take into account the initial states of the uncoupled lasers; the scenario is mainly determined by the ML operational regime and almost independent of the SL initial state. Each specific case of bistability is characterized by its own scenario in the route from uncorrelated motion to full correlation, as the coupling is increased. The cross-correlation analysis allowed us to discover regions with strong correlation for moderate coupling between a periodic ML and a quasiperiodic SL, i.e., the existence of a certain functional dependence between their oscillations, known as generalized synchronization. This regime may be useful for secure communication with bistable ECSLs. It our belief that many features of synchronization dynamics of the coupled ECSLs encountered in this work are inherent to a wider class of systems with coexisting attractors.

## ACKNOWLEDGMENT

This work was supported by Consejo Nacional de Ciencia y Tecnología de México (Project No. 46973).

[1] J. Maurer and A. Libchaber, J. Phys. (Paris), Lett. **41**, 515 (1980).
[2] D. M. Heffernan, Phys. Lett. **108A**, 413 (1985).
[3] J. M. T. Thompson and H. B. Stewart, *Nonlinear Dynamics and Chaos* (Wiley, Chichester, 1986).
[4] F. Ravelet, L. Marié, A. Chiffaudel, and F. Daviaud, Phys. Rev. Lett. **93**, 164501 (2004).
[5] J. -F. Vibert, A. S. Foutz, D. Caille, and A. Hugelin, Brain Res. **448**, 403 (1988); A. Hunding and R. Engelhardt, J. Theor. Biol. **174**, 401 (1995); E. M. Ozbudak, M. Thattai, H. N. Lim, B. I. Shraiman, and A. van Oudenaarden, Nature (London) **427**, 737 (2004).
[6] G. Jetschke, Phys. Lett. **72A**, 265 (1979); E. Laukina, J. Vidal-Gancedo, V. Laukin, J. Veciana, I. Chuev, V. Tkacheva, K. Wurst, and C. Rovira, J. Am. Chem. Soc. **125**, 3948 (2003).
[7] Zhang Yi and Kok Kiong Tan, IEEE Trans. Neural Netw. **15**, 329 (2004); S. A. Campbell, I. Ncube, and J. Wu, Physica D **214**, 101 (2006).
[8] A. Pikovsky, M. Rosenblum, and J. Kurths, *Synchronization: A Universal Concept in Nonlinear Science* (Cambridge University Press, New York, 2001).
[9] D. E. Postnov, T. E. Vadivasova, A. G. Balanov, and V. A. Anischenko, Chaos **9**, 227 (1999); B. P. Bezruchko, M. D. Prokhorov, and Ye. P. Seleznev, Chaos, Solitons Fractals **15**, 695 (2003); W. Uhm, V. Astakhov, A. Akopov, and S. Kim, Int. J. Bifurcation Chaos Appl. Sci. Eng. **17**, 4013 (2003).
[10] S. Yanchuk and T. Kapitaniak, Phys. Rev. E **64**, 056235 (2001).
[11] S. Guan, C.-H. Lai, and G. W. Wei, Phys. Rev. E **71**, 036209 (2005).
[12] A. N. Pisarchik, R. Jaimes-Reátegui, J. R. Villalobos-Salazar, J. H. García-López, and S. Boccaletti, Phys. Rev. Lett. **96**, 244102 (2006); A. N. Pisarchik, R. Jaimes-Reátegui, and J. H. García-López, Philos. Trans. R. Soc. London, Ser. A **366**, 459 (2008); Int. J. Bifurcation Chaos Appl. Sci. Eng. **18**, 1645 (2008).
[13] R. Roy and K. S. Thornburg, Jr., Phys. Rev. Lett. **72**, 2009 (1994); J. R. Terry, K. S. Thornburg, D. J. DeShazer, G. D. Vanwiggeren, S. Zhu, P. Ashwin, and R. Roy, Phys. Rev. E **59**, 4036 (1999).
[14] T. Sugawara, M. Tachikawa, T. Tsukamoto, and T. Shimizu, Phys. Rev. Lett. **72**, 3502 (1994); B. F. Kuntsevich and A. N. Pisarchik, Phys. Rev. E **64**, 046221 (2001).
[15] R. Meucci, F. Salvadori, M. V. Ivanchenko, K. A. Naimee, C. Zhou, F. T. Arecchi, S. Boccaletti, and J. Kurths, Phys. Rev. E **74**, 066207 (2006); A. Bergner, R. Meucci, K. A. Naimee, M. C. Romano, M. Thiel, J. Kurths, and F. T. Arecchi, *ibid.* **78**, 016211 (2008).
[16] L. Luo, P. L. Chu, T. Whitbread, and R. F. Peng, Opt. Commun. **176**, 213 (2000).
[17] C. R. Mirasso, P. Colet, and P. Garcia Fernandez, IEEE Photonics Technol. Lett. **8**, 299 (1996).

[18] K. A. Shore, P. S. Spencer, and I. Pierce, in *Recent Advances in Laser Dynamics: Control and Synchronization*, edited by A. N. Pisarchik (Research Signpost, Kerala, India, 2008).
[19] S. Sivaprakasam and K. A. Shore, Opt. Lett. **24**, 466 (1999).
[20] F. T. Arecchi, R. Meucci, G. Puccioni, and J. Tredicce, Phys. Rev. Lett. **49**, 1217 (1982).
[21] T. Baer, J. Opt. Soc. Am. B **3**, 1175 (1986).
[22] A. N. Pisarchik, Y. O. Barmenkov, and A. V. Kir'yanov, Phys. Rev. E **68**, 066211 (2003); IEEE J. Quantum Electron. **39**, 1567 (2003); J. M. Saucedo-Solorio, A. N. Pisarchik, A. V. Kir'yanov, and V. Aboites, J. Opt. Soc. Am. B **20**, 490 (2003).
[23] F. R. Ruiz-Oliveras and A. N. Pisarchik, Opt. Express **14**, 12859 (2006).
[24] R. Lang and K. Kobayashi, IEEE J. Quantum Electron. **16**, 347 (1980).
[25] C. Masoller and N. B. Abraham, Phys. Rev. A **57**, 1313 (1998).
[26] B. Krauskopf, in *Trends in Dynamical Systems*, edited by F. Dumortier, D. Roose, and A. Vanderbauwhede (Handelingen van de Koninklijke Vlaamse Academie van Belgie, Brussels, 2006), pp. 33–45.
[27] J. Ohtsubo, *Semiconductor Lasers—Stability, Instability and Chaos*, Springer Series in Optical Sciences (Springer-Verlag, Berlin, 2006).
[28] Yonggen Xu, Yude Li, Ting Feng, Yi Qiu, Fuxing Fu, and Wei Guo, J. Opt. Soc. Am. B **25**, 1303 (2008).
[29] V. V. Apollonov, S. I. Derzhavin, V. I. Kislov, V. V. Kuzminov, D. A. Mashkovsky, and A. M. Prokhorov, Opt. Express **4**, 19 (1999).
[30] V. Z. Tronciu, C. R. Mirasso, and P. Colet, J. Phys. B **41**, 155401 (2008).
[31] Shaoqing Wang, Xiangzhao Wang, Yingming Liu, and Yang Bu, J. Opt. Soc. Am. B **25**, 1350 (2008).
[32] P. Besnard, B. Meziane, and G. N. Stephan, IEEE J. Quantum Electron. **29**, 1271 (1993).
[33] M. Giudici, C. Green, G. Giacomelli, U. Nespolo, and J. R. Tredicce, Phys. Rev. E **55**, 6414 (1997).
[34] T. Heil, I. Fischer, W. Elsässer, B. Krauskopf, K. Green, and A. Gavrielides, Phys. Rev. E **67**, 066214 (2003).
[35] S. Erikson and A. M. Lindberg, J. Opt. B: Quantum Semiclassical Opt. **4**, 149 (2002); S. Wieczorek, T. B. Simpson, B. Krauskopf, and D. Lenstra, Opt. Commun. **215**, 125 (2003).
[36] S. Wieczorek, B. Krauskopf, and D. Lestra, Opt. Commun. **172**, 279 (1999).
[37] See EPAPS Document No. E-PLEEE8-78-105812 for a movie corresponding to Fig. 2. For more information on EPAPS, see http://www.aip.org/pubservs/epaps.html.